Faraday Discussions

Accepted Manuscript

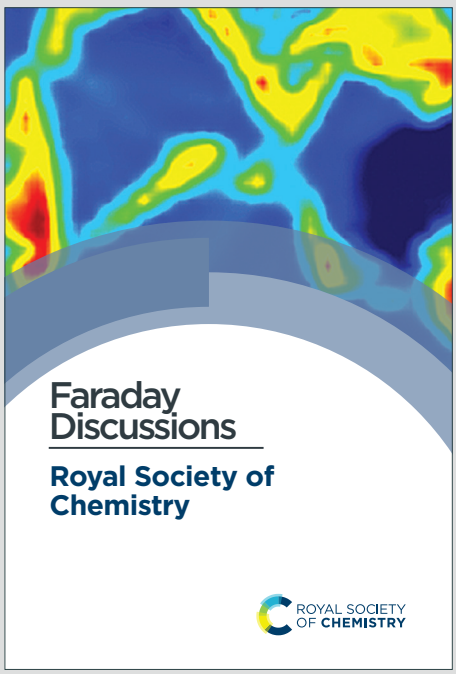

This article can be cited before page numbers have been issued, to do this please use: M. B. Karakaplan, V. S. Tiwari, O. Agazani, C. Echalier, G. Subra and M. Reches, *Faraday Discuss.*, 2024, DOI: 10.1039/D5FD00014A.

ROYAL SOCIETY OF CHEMISTRY

www.rsc.org/faraday_d

View Article Online
DOI: 10.1039/D5FD00014A

ARTICLE

Silylated peptides as building blocks for material synthesis using sol-gel polymerization

Received 00th January 20xx,
Accepted 00th January 20xx

DOI: 10.1039/x0xx00000x

Mehmet B. Karakaplan,[a,b] Vinay S. Tiwari,[a] Omer Agazani,[a] Cécile Echalier,[b] Gilles Subra,[b] and Meital Reches*[a]

The bottom-up approach exploits simple building blocks to generate new materials with desired physical and chemical characteristics. Here, we combine two bottom-up routes that occur under mild conditions, self-assembly and sol-gel synthesis, to program the shape and structure of materials. While self-assembly occurs through non-covalent interactions, sol-gel synthesis involves forming covalent bonds. As a proof of concept, we chose the self-assembled peptide Phe-Phe and its fluorinated analogue Phe(4-F)-Phe(4-F) to template the sol-gel process. These peptides were silylated to allow their self-mineralization. Scanning electron microscopy and atomic force microscope analysis revealed the formation of rod-shaped structures for the silylated Phe-Phe while spherical particles were formed by its fluorinated analogue. The size of the particles ranges from nano to micron scale. Fourier transform infrared spectrometry suggested the presence of parallel β-sheet secondary structure and siloxane bond formation that can stabilize these structures. Overall this approach can be adopted for other self-assembled peptides for generating new materials using a bottom-up approach.

Introduction

Precise control of material properties is essential for their successful application in diverse fields such as medicine[1], biomedical device[2], energy storage[3], coatings[4], and environmental technologies.[5] This entails the usage of a material synthesis strategy that can provide control over the smallest building blocks.[6] The bottom-up strategy is one of the best methods for the design and fabrication of new materials from the atomic to the micron scale. This strategy encompasses many approaches, such as self-assembly, polymerization, sol-gel, biosynthesis, and electrochemical deposition. This variety in fabrication methods provides materials with miscellaneous characteristics.[7]

Among these approaches, self-assembly has attracted great attention. The self-assembly process is driven by non-covalent interactions such as Van der Waals, π-π, and electrostatic interactions.[8] Self-assembly can result in the spontaneous formation of highly ordered structures at the nano and micron-scale.[9] This process can occur under mild conditions. Using different building blocks and altering the environmental conditions allows generating diverse architectures.[10]

Among these building blocks, peptides especially draw significant interest in creating self-assembled supramolecular structures due to their molecular recognition properties.[11–13] By designing various peptide sequences, it is possible to obtain versatile assemblies.[14–19] Self-assembling peptides are also excellent templates to initiate inorganic growth and mimic biomineralization.[20–22]

Another method to generate novel materials is by sol-gel synthesis. The sol-gel reaction starts with the hydrolysis of alkoxysilanes (Si-OR) into hydroxysilanes (Si-OH) and proceeds with the chemoselective condensation to form the siloxane (Si-O-Si) network of covalent bonds. One of the advantages of sol-gel synthesis is the ability to tailor the morphology, shape, and size of the materials by adjusting the solvent composition, pH, and precursor concentration.[23] Another way to control the structure of the materials is by structure-directing agents such as cetyltrimethylammonium bromide (CTAB).[24] Like self-assembly, sol-gel synthesis can be performed at room temperature.[25] The combination of these two fabrication methods can generate versatile materials with different characteristics.

Here, we combine self-assembly and sol-gel synthesis for making novel materials using a one-pot method. As a proof of principle, we used the dipeptide Phe-Phe, a well-known self-recognition element, and its fluorinated analogue Phe(4-F)-Phe(4-F). 3-isocyanatopropyltriethoxysilane (ICPTES) was used to silylate the peptides on their free amino groups (N-terminal). The silylated peptides were used as a precursor for material synthesis in aqueous acidic conditions (pH=1.5). These conditions favour the hydrolysis of ethoxysilanes into the

[a] Institute of Chemistry and The Center for Nanoscience and Nanotechnology, The Hebrew University of Jerusalem, Jerusalem 91904, Israel
[b] IBMM, Université de Montpellier, CNRS, ENSCM, 34293 Montpellier, France
*Correspondence to: meital.reches@mail.huji.ac.il
Supplementary Information available: [details of any supplementary information available should be included here]. See DOI: 10.1039/x0xx00000x

View Article Online
DOI: 10.1039/D5FD00014A

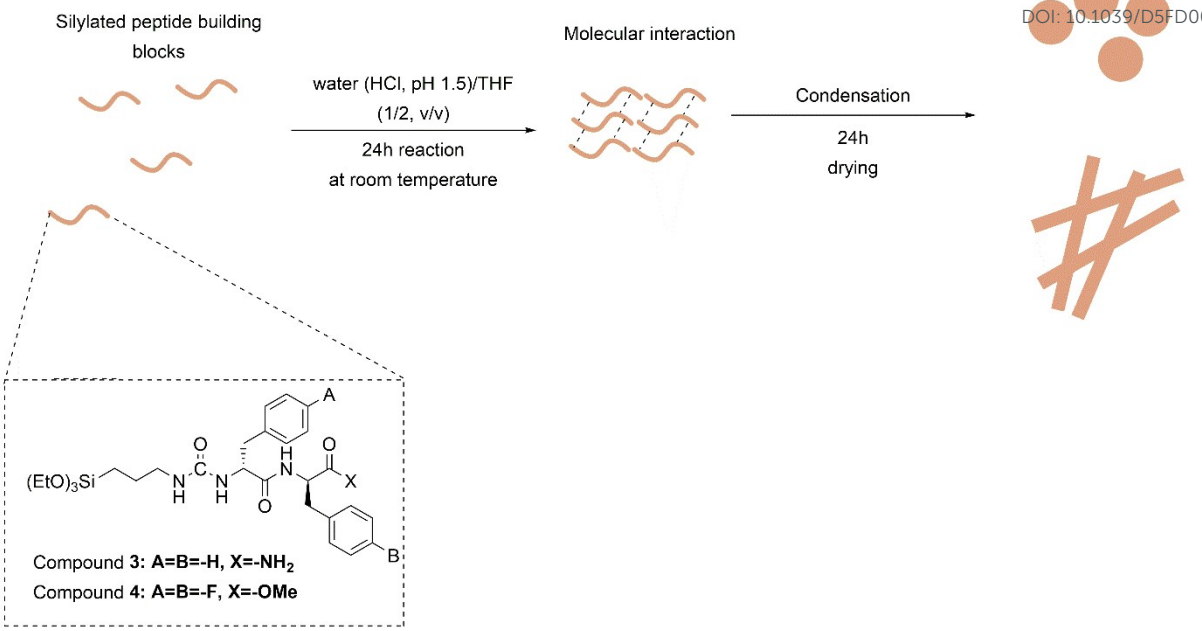

Figure 1. Schematic representation of material synthesis from silylated peptide building blocks. The proposed mechanism involves the hydrolysis of the silylated peptides followed by their condensation driven by self-assembly.

hydroxysilanes but prevent the spontaneous formation of siloxane bonds at low concentrations. However, the molecular recognition among the dipeptides drives the structural organization of the system by bringing the silanol groups to proximity and favouring their condensation. Based on this mechanism, the silane groups on peptides can "freeze" the structure covalently and provide stability. This simple concept can pave the way for designing materials that are driven by self-assembly but stabilized by covalent bonds.

Experimental Section

Material

All solvents and reagents were used as supplied. Solvents used for high-performance liquid chromatography (HPLC) were HPLC grade. N-N'-dimethylformamide (DMF), acetonitrile (ACN), trifluoroacetic acid (TFA), tetrahydrofuran (THF), diethyl ether, and diisopropylethylamine (DIEA) were purchased from Bio-Lab (Jerusalem, Israel). Triple distilled water (TDW) was obtained through a Milli-Q water filtering system (Millipore). 3-(Triethoxysilyl)propyl isocyanate (ICPTES) was obtained from Thermo Fisher Scientific (Lancashire, UK). Copper grids (pure carbon film 400 mesh) were purchased from Ted Pella Inc. (Redding, CA).

Silylation of peptides

One equiv. of peptide **1** or **2** was completely dissolved in 1 mL DMF at a concentration of 0.2 M. DIEA (4.5 equiv.) was added to the reaction and stirred for 5 min. Lastly, ICPTES (2 equiv.) was added to the reaction mixtures and stirred for 2 hours under argon. At the end of the reaction, the silylated peptides (compound **3** and compound **4**) were precipitated by adding 30 mL of diethyl ether and centrifuged. The pellet was resuspended in fresh diethyl ether and centrifuged thrice in total. The pellet was dried under vacuum overnight and kept at +4 °C with argon for further use (Scheme 1).[20]

Material synthesis

Compounds **3** and **4** were separately dissolved in a mixture of TDW (HCl, pH 1.5)/THF (1/2, v/v) at two different concentrations, 1.78 mM and 17.80 mM, resulting in four distinct reactions. After a short sonication, the reactions were stirred for 24 hours at room temperature. The solvent mixtures were evaporated overnight in a fume hood to induce the condensation reaction. The obtained white products were washed 3 times with water (HCl, pH 1.5) and dispersed in TDW for further use. The concentration of 17.80 mM was selected based on our findings from a previous study.[20] The initially published concentration (38.5 mM) led to rapid gelation and condensation for compounds **3** and **4**. To obtain dispersed particles, the concentration was lowered by half to 17.80 mM. Furthermore, to investigate the effect of significantly lower concentration on material architecture and size, 10 times diluted concentration (1.78 mM) was employed for material synthesis.

High-performance liquid chromatography (HPLC)

Samples (peptide **1**, peptide **2**, compound **3**, and compound **4**) for HPLC were dissolved in ACN/TDW (50:50, v/v) including 0.1% TFA at 2 mg/mL concentration. The analysis was performed

using a Waters Alliance reverse-phased analytical HPLC with an XSelect C18 column (3.5 µm 130 Å, 4.6 × 150 mm). UV detection was performed at 220 nm and 254 nm. A linear gradient (5% to 95%) of ACN (with 0.1% TFA) in TDW (with 0.1% TFA) was used to elute the peptides and silylated peptides at a flow rate of 1 mL/min**.** Peptide **2** was eluted with a linear gradient (30% to 95%) of ACN with (0.1% TFA) in TDW (with 0.1% TFA).

Mass spectroscopy (MS)

The mass analysis (for peptide **1**, peptide **2**, compound **3**, and compound **4**) was performed by electron spray ionization mass spectroscopy using a SCIEX Triple Quad 3500 (Framingham, MA, USA). The results were analysed via SCIEX Analyst software.

Scanning transmission electron microscopy (STEM)

A drop of 10 µL from the material dispersions in TDW (1 mg/mL) was placed on a clean silicon substrate or copper grids and dried under vacuum. STEM images were recorded using an analytical high-resolution scanning electron microscope Apreo 2S (Thermo Fisher Scientific, OR, USA) with 2 - 20 kV acceleration voltage, current of 0.1 - 0.4 nA, and 4 - 10 mm working distance.

Atomic force microscopy (AFM)

The material dispersions were drop-casted on a clean silicon wafer. All the AFM images were taken at AC mode with Si_3N_2 tip with a spring constant of 3 N m^{-1} by JPK NanoWizard3® (Berlin, Germany).

Dynamic light scattering (DLS)

The hydrodynamic diameter of the materials was measured by a Zetasizer Nano ZS DLS instrument (Malvern Instruments, UK). The material suspensions were prepared in TDW at a concentration of 1 mg/mL. For accurate measurements, they were sonicated for 20 min and vortexed for 1 min after adding 10 µL of Tween 80. The measurements were carried out three times and standard deviations were included.

Attenuated total reflectance (ATR) Fourier transform infrared (FTIR) spectrometry

White powder samples (**N3H**, **N3L**, **N4H**, and **N4L**) were analysed via ATR-FTIR spectrometer (Alpha II, Bruker Optics GmbH). The measurements were taken at 1 cm^{-1} resolution and 10 scans.

X-ray diffraction (XRD) analysis

The phases of the materials (**N3H**, **N3L**, **N4H**, and **N4L**) were identified by powder XRD (X-Ray Diffractometer - D8 Advance, Bruker) (2θ=10-50°, at a step size of 0.02 deg sec^{-1}) using Cu Kα (λ=0.15406 nm) and solid state NaI dynamic scintillation detector. The data was analysed via FullProf Suite software.

Results and discussion

Peptide **1** and peptide **2** were synthesized via liquid-phase peptide synthesis (LPPS). See the Scheme S1 in the ESI†. Peptide **1** (*H-Phe-Phe-NH_2*) was synthesized with a purity of 99% according to the HPLC analysis (Figure S1A in the ESI†). The molecular weight was confirmed with MS (m/z=312), $(M + H)^+$ = 312.3 (Figure S1B in the ESI†). Silylation of peptide **1** yielded compound **3**. Compound **3** was analysed using HPLC and MS (m/z = 475.19, $(M + H)^+$ = 475) to confirm its identity (Figure S3 in the ESI†). After dissolving compound **3** at the concentrations of 1.78 mM or 17.80 mM in TDW (HCl, pH 1.5)/THF (1/2, v/v) solvent mixture, the reactions were stirred for 24 hours. Then, the solvents were evaporated for an additional 24 hours. See the Figure 1. After solvent evaporation, the obtained white solid materials were washed with TDW (HCl, pH 1.5) three times. The obtained white solid materials were noted as **N3L** for 1.78 mM and **N3H** for 17.80 mM. At 1.78 mM, the reaction remained clear for 24 hours suggesting that the sol-gel condensation did not proceed. Indeed, at pH 1.5, the hydrolysis of triethoxysilane is fast whereas the condensation is unfavourable. In this case, condensation was induced by the evaporation of the solvents.

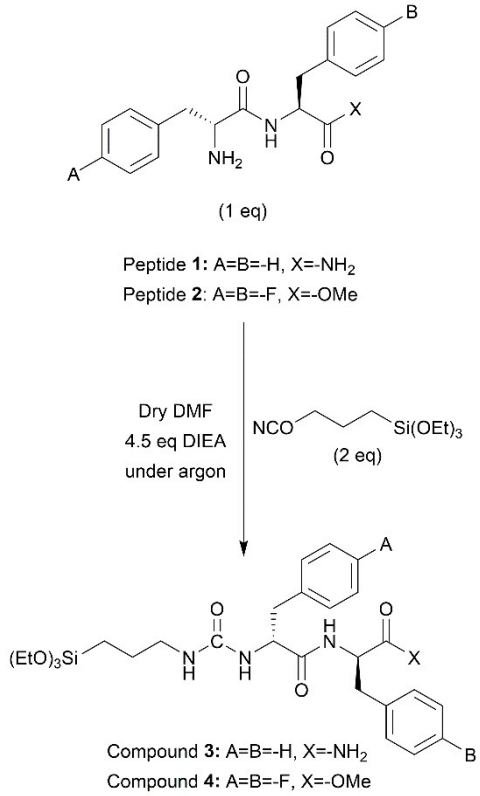

Scheme 1. Synthesis of compound **3** and compound **4**

The formation of **NH3** displays the same principle as **N3L**. Differently, **N3H** showed a slight turbidity, compared to **N3L**, a few hours after the initiation of the reaction. This can be explained by the fast self-assembly and condensation due to the high concentration of compound **3**. Moreover, when the concentration was above 17.80 mM, the precursors rapidly condensed and generated a gel-like structure and therefore the concentration was adjusted to obtain dispersions rather than gels. As shown in Figures 2A and 2G, SEM analysis revealed that

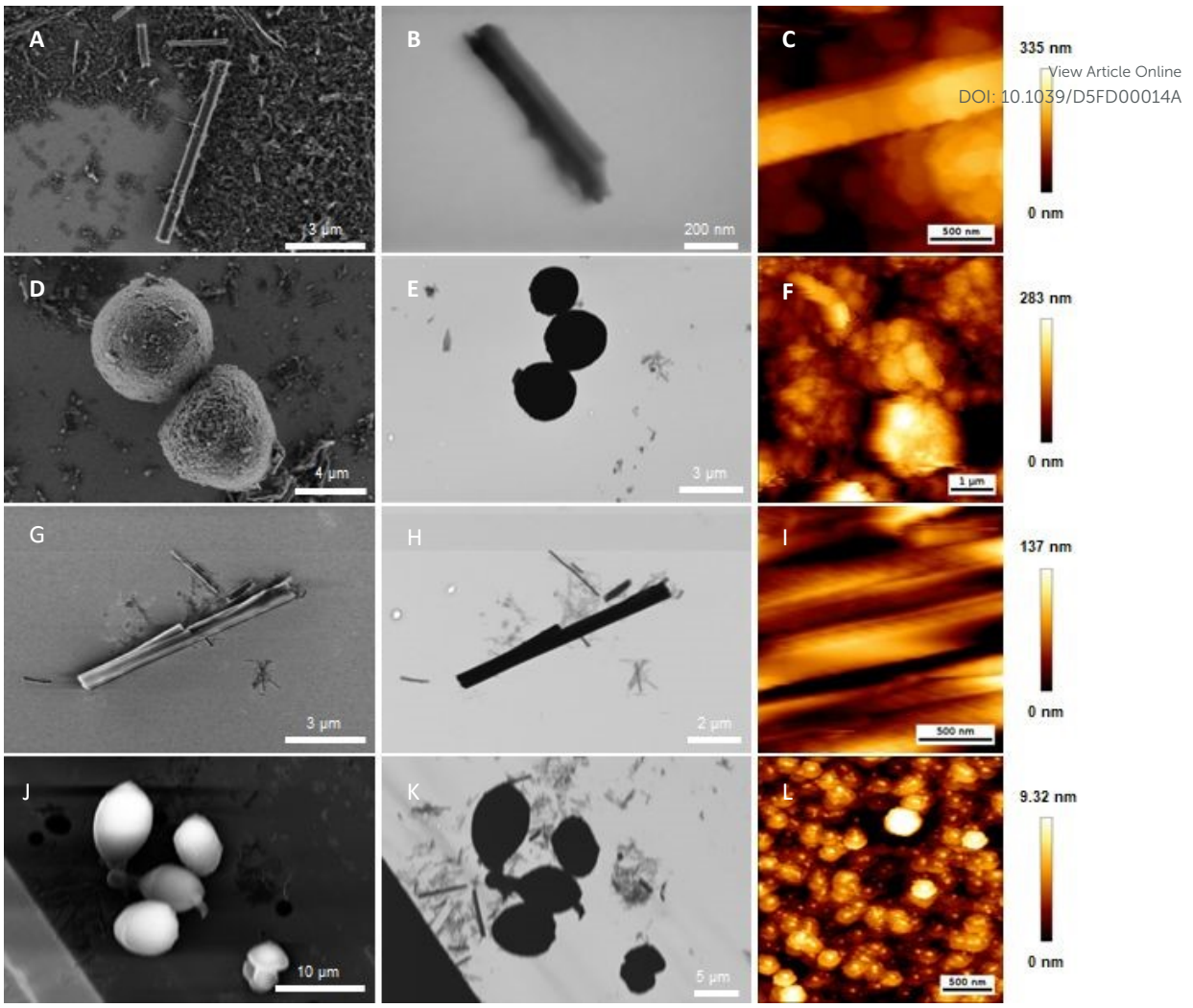

Figure 2. Structural characterization of the materials formed by combining self-assembly and sol-gel process. A) SEM, B) STEM and C) AFM representative images of the materials formed by **N3H**, D) SEM, E) STEM and F) AFM of **N4H**, G) SEM, H) STEM, and I) AFM representative images of the materials formed by **N3L**, and J) SEM, K) STEM and L) AFM representative images of the materials formed by **N4L**.

N3H and **N3L** are rod-shaped materials with ranging sizes. In Table 1, DLS analysis demonstrated that the polydispersity index (PDI) for **N3H** is high. This means that **N3H** has a broad size particle distribution from nano to micron scale. Although the average size for **N3H** was 582.4 nm ± 18.7, low-magnification SEM images showed the presence of micron-scale particles (Figure S5A in the ESI†). **N3L** had a relatively larger average size than **N3H**. However, the PDI value was smaller than **N3H**, which means it has a narrower size distribution.

Peptide **2** (*H-Phe(4-F)-Phe(4-F)-OMe*) was synthesized with a purity of 98% (Figure S2A in the ESI†) and analysed by MS (m/z = 363), $(M + H)^+$ = 362.7 (Figure S2B in the ESI†). Following the synthesis, peptide **2** was reacted with 2 equiv. of ICPTES to yield compound **4**. Compound **4** was characterized by HPLC (Figure S4A in the ESI†) and its purity was 86%. Once the identity of compound **4** was confirmed with MS (m/z = 525.17), (M + H = 525) (Figure S4B in the ESI†), it was used for the material synthesis by combining self-assembly and sol-gel process. Two different concentrations of compound **4** were dissolved in a mixture of TDW (HCl, pH 1.5)/THF (1/2, v/v), at 1.78 mM and 17.80 mM. At 1.78 mM, the reaction remained clear for 24 hours suggesting that the sol-gel reaction did not proceed as in the case of **N3L.** After solvent evaporation, **N4L** was recovered as a solid precipitate and analysed using STEM. Figure 2D and 2J, show the formation of ovoid-shaped materials by **N4H** and **N4L**. These structures by **N4L** and **N4H** are in the nano and micron scale. The particles formed by **N4H** showed a wide range of size distribution to the extent that, SEM images of **N4H** demonstrated particles from the nanoscale to microscale (Figure S5B in the ESI†). On the other hand, similar to **N3L**, **N4L** has a narrower size distribution with 0.301 PDI.

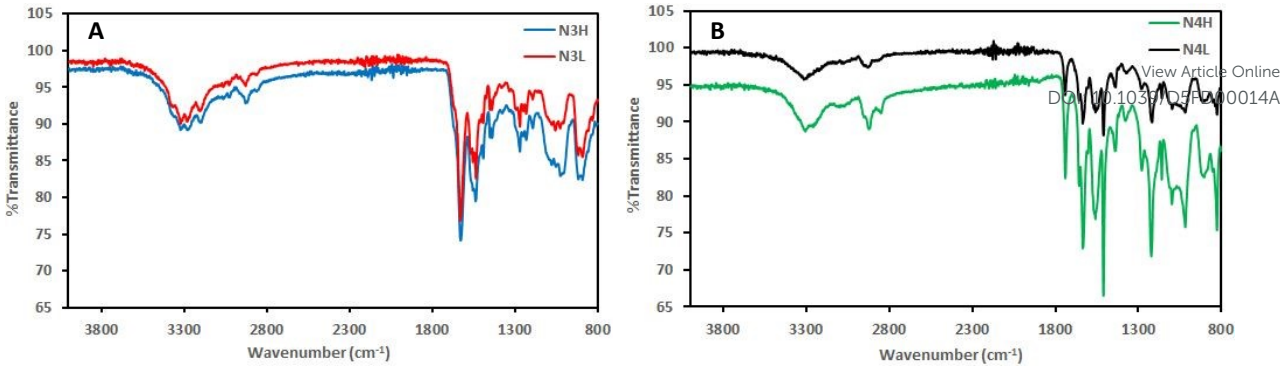

Figure 3. FTIR spectrum of A) **N3H** (blue), **N3L** (red) B) **N4H** (green) and **N4L** (black).

Table 1. The average size and polydispersity index (PDI) values for the materials were determined by DLS.

Material	Z-Average (nm)	PDI (AU)
N3H	582.4 ± 18.7	0.444 ± 0.02
N3L	842.7 ± 41.3	0.252 ± 0.03
N4H	612.3 ± 68.2	0.695 ± 0.09
N4L	768.1 ± 40.9	0.301 ± 0.11

In nanomaterial synthesis, it is generally expected that as the concentration of the precursor increases, larger particles are obtained.[26,27] Although the average size (obtained by DLS) of higher reaction concentrations (**N3H** and **N4H**) is relatively smaller than lower reaction concentrations (**N3L** and **N4L**), we could not detect a large difference in size using STEM analysis (Figure 2B, 2E, 2H, and 2K). This can be due to the high polydispersity of the particles that resulted in misleading values by DLS.[28] However, it can be noted from the PDI values that lower reaction concentration can provide better size uniformity (Table 1). These results were confirmed by the AFM for **N4H** and **N4L**. The nano-scale spheres of **N4H** aggregated into micron-level agglomerates (Figure 2F), while **N4L** created separated and uniform spheres (Figure 2L). AFM morphology analysis of **N3H** (Figure 2F) and **N3L** were consistent with STEM and TEM images.

ATR-FTIR spectrometry was used to analyse the secondary structures and siloxane bonds. As expected, **N3H** and **N3L** have very similar spectra (Figure 3A). This suggests that the different reaction concentrations did not affect the chemical structure of these materials. The characteristic peak for siloxanes falls within the range between 1000 and 1200 cm^{-1}.[29] The band at 1028 cm^{-1} is associated with linear siloxane bonds.[30] Besides, Si–O–Si asymmetric stretching was observed at 1056 cm^{-1} which is seen in the strained geometry.[31] The peaks and 1056 and 1080 cm^{-1} also represent the Si-O-C vibrations.[20,30] In addition, amide II (N-H) at 1560 cm^{-1} arises primarily from N-H bending[32]. The peak at 1632 cm^{-1} is attributed to amide I (C=O) in the material[33] and also suggests a β-sheet structure.[34,35] The distance between amide II and amide I ($\Delta\nu$) is a good indication of the strength of the hydrogen bonds. The lower $\Delta\nu$ value demonstrates the stronger hydrogen bonds. In a study that is reported by Jebors et al., $\Delta\nu$ is around 90 which addresses the strong hydrogen bonding.[20] For **N3H** and **N3L**, $\Delta\nu$ value was 72 suggesting the formation of a secondary structure of a parallel β-sheet.[36]

For **N4H** and **N4L**, we observed a sharp peak that represents the siloxane bond at 1150 cm^{-1} and another sharp peak that represents the silica network at 825 cm^{-1}.[37,38] Additionally, we observed a band at 1737 cm^{-1} that represents methyl ester peptide **2**. Since peptide **2** is composed of a fluorinated analogue we observe a sharp peak at 1220 cm^{-1} for the C-F bond on the benzene ring. Differently, **N4H** and **N4L** showed a peak at 3305 cm^{-1} that was attributed to free -OH of hydroxysilanes. Amide II and amide I were visible at 1561 cm^{-1} and 1633 cm^{-1}, respectively. Same as **N3H** and **N3L**, $\Delta\nu$ for these materials is 72 which shows strong hydrogen bonds. This also suggests a parallel β-sheet secondary structure in the amide I band at 1630 cm^{-1} like **N3L**.[36] Antiparallel β-sheets give a small peak at 1694 cm^{-1} which was not observed for any of the other materials.[39] This would be compatible with a mechanism in which parallel β-sheet formation brought in proximity the N-terminal of compound **3** and **4** and provide them to condense. Additionally, all materials showed common peaks such as ~2930 and ~2850 cm^{-1} for N-H stretching, ~1450 cm^{-1} N-H deformations of urea, and ~1555 cm^{-1} for C=C from phenyls.

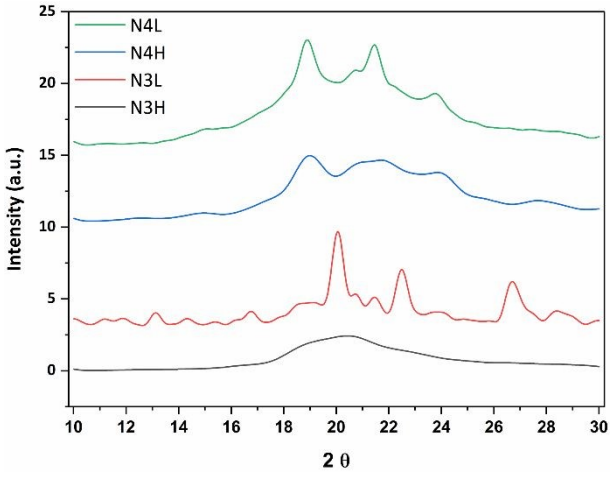

Figure 4. XRD patterns of **N3H** (black), **N3L** (blue), **N4H** (red), and **N4L** (green).

XRD analysis was performed to analyse the phases of materials. All materials (**N3H**, **N3L**, **N4H**, and **N4L**) showed a broad diffraction peak centred at 20.4°, typical for amorphous silica.[40] See the Figure 4. Differently, we observed diffraction peaks at 20°, 22.5°, and 26.7° for **N3L**. Although **N3L** exhibited an amorphous phase, its diffraction peaks at 20°, 22.5°, and 26.7° corresponded to those observed in diphenylalanine peptide assemblies, as reported in a study by Ji et al.[41] **N4H** and **N4L** showed a similar pattern in XRD analysis and they were amorphous.

Conclusions

Peptides provide simple building blocks for generating new materials through a bottom-up approach termed self-assembly. This process yields various architectures by non-covalent interactions formed under mild conditions. These architectures can assemble only under specific conditions and their stability can be disrupted when the conditions change. Here, we demonstrated the combination of self-assembly with another bottom-up approach, sol-gel synthesis. Sol-gel synthesis includes the formation of covalent siloxane bonds that can stabilise the resulting assemblies. We demonstrated the combination of self-assembly and sol-gel synthesis utilising the peptide diphenylalanine and its fluorinated analogue. These two peptides were silylated and used to template the growth of a sol-gel condensation reaction. Rod-shaped and spherical structures were formed by this approach. Their size ranges from the nano to the micron scale. FT-IR spectra of the materials indicated the presence of parallel β-sheet secondary structures and siloxane bond formations. Overall, the combination of these two bottom-up approaches, self-assembly and sol-gel, can provide a novel method for generating stable materials with miscellaneous characteristics in terms of shape, size, and morphology.

Author contributions

We strongly encourage authors to include author contributions and recommend using CRediT for standardised contribution descriptions. Please refer to our general author guidelines for more information about authorship.

Conflicts of interest

There are no conflicts to declare.

Data availability

The raw data of this publication are available on the Dataverse website at the link: https://dataverse.unimi.it/dataverse/HUJI-UM-MBK-1. The details of experimental procedures are provided in the electronic supplementary information (ESI)†.

Acknowledgements

This project received funding from the European Union's research and innovation programme under the Marie Sklodowska-Curie grant agreement No. 101072645.

References

1 M. Vallet-Regí, M. Colilla and B. González, *Chem. Soc. Rev.*, 2011, **40**, 596–607.

2 W. Park, H. Shin, B. Choi, W.-K. Rhim, K. Na and D. Keun Han, *Progress in Materials Science*, 2020, **114**, 100686.

3 X. Zhao, Z. Li, Q. Guo, X. Yang and G. Nie, *Journal of Alloys and Compounds*, 2021, **855**, 157480.

4 I. Zvonkina and M. Soucek, *Current Opinion in Chemical Engineering*, 2016, **11**, 123–127.

5 M. Ş. A. Eren, H. Arslanoğlu and H. Çiftçi, *Journal of Environmental Chemical Engineering*, 2020, **8**, 104247.

6 U. Ulusoy, *Minerals*, 2023, **13**, 91.

7 L. V. Srinivasan and S. S. Rana, *Discov Appl Sci*, 2024, **6**, 371.

8 J. Wang, K. Liu, R. Xing and X. Yan, *Chem. Soc. Rev.*, 2016, **45**, 5589–5604.

9 R. Chang, C. Yuan, P. Zhou, R. Xing and X. Yan, *Acc. Chem. Res.*, 2024, **57**, 289–301.

10 C. Yuan, Q. Li, R. Xing, J. Li and X. Yan, *Chem*, 2023, **9**, 2425–2445.

11 F. Fan, X. Chen, J. Lin, M. Lin, L. Li, Y. Gu, Y. Chai, H. Zhang, X. Chen and Q. Li, *Adv Funct Materials*, 2024, **34**, 2470125.

12 R. Xing, C. Yuan, W. Fan, X. Ren and X. Yan, *Sci. Adv.*, 2023, **9**, eadd8105.

13 C. Yuan, W. Fan, P. Zhou, R. Xing, S. Cao and X. Yan, *Nat. Nanotechnol.*, 2024, **19**, 1840–1848.

14 D. Mandal, A. Nasrolahi Shirazi and K. Parang, *Org. Biomol. Chem.*, 2014, **12**, 3544–3561.

15 G. Ghosh, R. Barman, A. Mukherjee, U. Ghosh, S. Ghosh and G. Fernández, *Angew Chem Int Ed*, 2022, **61**, e202113403.

16 S. Yuran, Y. Razvag and M. Reches, *ACS Nano*, 2012, **6**, 9559–9566.

17 Z. Jin, Y. Li, K. Li, J. Zhou, J. Yeung, C. Ling, W. Yim, T. He, Y. Cheng, M. Xu, M. N. Creyer, Y. Chang, P. Fajtová, M. Retout, B. Qi, S. Li, A. J. O'Donoghue and J. V. Jokerst, *Angew Chem Int Ed*, 2023, **62**, e202214394.

18 S. Maity, S. Nir, T. Zada and M. Reches, *Chem. Commun.*, 2014, **50**, 11154–11157.

19 M. Kaganovich, K. Shlosman, E. Goldman, M. Benchis, T. Eitan, R. Shemesh, A. Gamliel and M. Reches, *Microbe Killer Polymeric Films Made by Melt-Compounding and Compression of Peptide Assemblies and Polyethylene*, In Review, 2022.

20 S. Jebors, L. Valot, C. Echalier, B. Legrand, R. Mikhaleff, A. Van Der Lee, R. Arenal, P. Dumy, M. Amblard, J. Martinez, A. Mehdi and G. Subra, *Mater. Horiz.*, 2019, **6**, 2040–2046.

21 M. C. Mañas-Torres, G. B. Ramírez-Rodríguez, J. I. García-Peiro, B. Parra-Torrejón, J. M. Cuerva, M. T. Lopez-Lopez, L. Álvarez De Cienfuegos and J. M. Delgado-López, *Inorg. Chem. Front.*, 2022, **9**, 743–752.

22 S. Jebors, S. Cecillon, C. Faye, C. Enjalbal, M. Amblard, A. Mehdi, G. Subra and J. Martinez, *J. Mater. Chem. B*, 2013, **1**, 6510.

23 M. Catauro and S. V. Ciprioti, *Materials*, 2021, **14**, 1788.

24 D. Desai, D. S. Karaman, N. Prabhakar, S. Tadayon, A. Duchanoy, D. M. Toivola, S. Rajput, T. Näreoja and J. M. Rosenholm, *Open Material Sciences*, DOI:10.2478/mesbi-2014-0001.

25 D. Bokov, A. Turki Jalil, S. Chupradit, W. Suksatan, M. Javed Ansari, I. H. Shewael, G. H. Valiev and E. Kianfar, *Advances in Materials Science and Engineering*, 2021, **2021**, 5102014.

26 S. Stopic, F. Wenz, T.-V. Husovic and B. Friedrich, *Metals*, 2021, **11**, 463.

27 M.-Z. Yu, J.-Z. Lin and T.-L. Chan, *Chemical Engineering Science*, 2008, **63**, 2317–2329.

28 E. Tomaszewska, K. Soliwoda, K. Kadziola, B. Tkacz-Szczesna, G. Celichowski, M. Cichomski, W. Szmaja and J. Grobelny, *Journal of Nanomaterials*, 2013, **2013**, 313081.

29 T. Hayeri and V. Mannari, *J Coat Technol Res*, 2025, **22**, 225–237.

30 M. Masmoudi, C. Rahal, M. Abdelmouleh and R. Abdelhedi, *Applied Surface Science*, 2013, **286**, 71–77.

31 H. Mori, Y. Miyamura and T. Endo, *Langmuir*, 2007, **23**, 9014–9023.

32 N. Ardila, F. Daigle, M.-C. Heuzey and A. Ajji, *Molecules*, 2017, **22**, 100.

33 Z. Ma, Y. Hong, D. M. Nelson, J. E. Pichamuthu, C. E. Leeson and W. R. Wagner, *Biomacromolecules*, 2011, **12**, 3265–3274.

34 G. Zandomeneghi, M. R. H. Krebs, M. G. McCammon and M. Fändrich, *Protein Sci*, 2004, **13**, 3314–3321.

35 J. P. Lomont, J. S. Ostrander, J.-J. Ho, M. K. Petti and M. T. Zanni, *J Phys Chem B*, 2017, **121**, 8935–8945.

View Article Online
DOI: 10.1039/D5FD00014A

36 L. P. DeFlores, Z. Ganim, R. A. Nicodemus and A. Tokmakoff, *J. Am. Chem. Soc.*, 2009, **131**, 3385–3391.

37 A. Issa and A. Luyt, *Polymers*, 2019, **11**, 537.

38 Y.-S. Li and A. Ba, *Spectrochimica Acta Part A: Molecular and Biomolecular Spectroscopy*, 2008, **70**, 1013–1019.

39 K. Zhaliazka and D. Kurouski, *ACS Chem Neurosci*, 2022, **13**, 2813–2820.

40 P. Lu and Y.-L. Hsieh, *Powder Technology*, 2012, **225**, 149–155.

41 W. Ji, Y. Tang, P. Makam, Y. Yao, R. Jiao, K. Cai, G. Wei and E. Gazit, *J. Am. Chem. Soc.*, 2021, **143**, 17633–17645.

View Article Online
DOI: 10.1039/D5FD00014A

Data availability statement

The raw data of this publication are available on the Dataverse website at the link: https://dataverse.unimi.it/dataverse/HUJI-UM-MBK-1. The details of experimental procedures are provided in the electronic supplementary information (ESI).